applied sciences

MDPI

Study Protocol

Support Patterns of Roadways Under Fractured Surrounding Rocks Based on the Quality Level of Rock Mass

Chi Ma [1], Peitao Wang [1,*], Jiajun Li [1], Xingwang Fan [1], Zhihong Dong [1], Ziming Chen [1] and Xingwu Wang [2]

[1] School of Civil and Resource Engineering, University of Science and Technology Beijing, Beijing 100083, China; machi@xs.ustb.edu.cn (C.M.); m202220142@xs.ustb.edu.cn (J.L.); m202320072@xs.ustb.edu.cn (X.F.); b20190006@xs.ustb.edu.cn (Z.D.); m202320150@xs.ustb.edu.cn (Z.C.)
[2] Hainan Mining Co., Ltd., Haikou 571927, China; m202320130@xs.ustb.edu.cn
* Correspondence: wangpeitao@ustb.edu.cn

Abstract: The roadway project of broken rock mass in the Shilu Iron Deposit was taken as the research object to discuss the stability control of the surrounding rocks using support patterns with broken rock mass. The grade evaluation of rock mass quality was conducted based on the geomechanical classification of rock mass. The roadway support effect in broken rock mass was calculated. Then, the section convergence characteristics of roadway surrounding rocks were analyzed under the current support scheme using displacement monitoring technology. The conclusions were described as follows: (1) The surrounding rock integrity of the No.6 and No.7 transportation roadways in the middle section of the Baoxiu mining area (Level 120) is poor. Based on geological survey data and rock mass classification, the rock mass quality in this region has been rated as Class IV. The joint support pattern of the anchor net and shotcrete was used according to the support guidelines. (2) The parameters for the support structure within Shilu Iron Deposit were designed, according to the requirements, as follows: the use of Portland cement; a shotcrete thickness of 55 mm; resin bolts with a minimum outer diameter of φ 20 mm and a length of 2200 mm; and row and column spacings of 1100 mm each. Meanwhile, a rectangular metal mesh of 80 × 80 mm was used as the anchor mesh. (3) The cross-section displacement reached 20 mm within a week using the support pattern according to displacement monitoring results of the on-site roadway section. Moreover, the convergence deformation rate significantly changed. However, the rate rapidly decreased after the first week, and the cross-section showed no further deformation after one month. The support pattern could control the displacement of surrounding rocks, which was verified by the monitoring results.

Keywords: broken surrounding rocks; support pattern; joint support; surrounding rock stability

check for updates

Citation: Ma, C.; Wang, P.; Li, J.; Fan, X.; Dong, Z.; Chen, Z.; Wang, X. Support Patterns of Roadways Under Fractured Surrounding Rocks Based on the Quality Level of Rock Mass. *Appl. Sci.* **2024**, *14*, 10598. https://doi.org/10.3390/app142210598

Academic Editor: Ricardo Castedo

Received: 26 September 2024
Revised: 9 November 2024
Accepted: 13 November 2024
Published: 17 November 2024

Copyright: © 2024 by the authors. Licensee MDPI, Basel, Switzerland. This article is an open access article distributed under the terms and conditions of the Creative Commons Attribution (CC BY) license (https://creativecommons.org/licenses/by/4.0/).

1. Introduction

Rock masses and deposits with poor geological structure or ore body conditions are frequently encountered in the pursuit of deep mineral resources, including broken surrounding rock deposits [1], high-temperature deposits, and flammable deposits [2]. Broken rock mass is a common complex geological body with low strength, well-developed fracture structures, and poor stability. Roadways within broken rock mass are susceptible to roof caving, rib spalling, and collapses. Therefore, the long-term stability of roadways with broken rock mass is of great significance to deep underground engineering [3–5].

Huang et al. [6] evaluated the deformation profiles of surrounding rock mass at varying distances from the broken zone to understand the instability of broken rock mass. The deformation of surrounding rock mass within and adjacent to the broken zone is explored via on-site measurements, theoretical research, and numerical simulations. Huang et al. [7] integrated the program with the unique unit modeling platform to generate an equivalent model of broken rock mass based on DFN-DEM coupling technology. A numerical compression test was conducted on the cylindrical rock sample prepared by the proposed

simulation method to determine the REV size of the target rock mass at Liyang Power Station. Zhao et al. [8] analyzed the geological characteristics, damage types, influencing factors, and support types of the broken rock mass roadway of Xinli Gold Mine. The Q system, RMR, and GSI are used to obtain the rock mass grading and physical and mechanical parameters. The surrounding rock partition, stability analysis, and support scheme design are conducted based on the rock mass grading results.

Niu et al. [9] proposed a new method for the scientific and rational characterization of complex cracks in the stability analysis of roadway surrounding rocks. The method addresses the challenges posed by cracks in the surrounding rock of deeply buried roadways under complex geological conditions. On-site measurements are combined with numerical simulations and physical experiments to provide a strong ability for comprehensive analysis. Yu et al. [10] focused on the 790 m horizontal section in Jinchuan Mine II for their research. They investigated the formation and evolution law of the fracture zone in the surrounding rock and proposed strategies that minimize the initial cracking zone and halt its growth. Yao et al. [11] designed a roadway reinforcement consisting of wet shotcreting and bolt support. The proportion of wet shotcreting is determined in industrial tests. Zhou et al. [12] optimized the support form and parameter selection for roadways in deep mining areas based on the calculation results of Flac3D simulation software. Zhang et al. [13] analyzed the failure causes of roadway support in a deep copper mine. The roadway support in the broken area is optimized based on the calculation results of the broken ring radius and stress distribution, which achieves positive engineering results. Yang et al. [14] systematically evaluated the existing support patterns in the Jinchuan mining area. Four different support schemes are proposed based on the on-site support failure. The schemes are applied to the operations of mining areas to control the deformation of the surrounding rock in the high-stress broken rock mass.

Extensive research has been conducted on the stability control of roadway-surrounding rocks. However, technologies for controlling roadway stability with deep broken rock mass remain imperfect. The rock mass support pattern is determined through the quality evaluation of deep rock mass, with Shilu Iron Deposit serving as the research background. The stability of roadway surrounding rocks is analyzed to design the optimal support pattern based on numerical simulation experiments and on-site monitoring. This pattern provides a valuable reference for the mining of similar broken deposits.

2. Project Profile

Shilu Iron Deposit, including the Beiyi and Baoxiu quarries, is located in Changjiang, Hainan Province, China. The underground mining method is non-pillar sublevel caving. The Beiyi quarry is an open-air-to-underground quarry, while the Baoxiu mining area is an underground quarry (Figure 1). The local areas of the eastern Beiyi district and Baoxiu district are greatly affected by extensive fracture structures according to the disclosure on the roadways developed within Shilu Iron Deposit. Especially, No.6–7 transportation roadways in the middle section of Baoxiu-120 exhibit poor rock integrity, characterized by crisscrossed cracks and a high weathering degree. The lithology is mainly pyroxene, amphibolite, and dolomite, with minor occurrences of phyllite, quartz, and epidote, exhibiting strong metasomatism. The minerals are arranged in a banded pattern, typical of silica-type deposits. Surrounding rocks are broken in the local mining area due to large-scale fracture structures (Figure 2).

Most support technologies rely on empirical designs, often resulting in suboptimal performance. For example, rib spalling and roof caving are prevalent issues in supported areas, with rib spalling observed in transport roadway No.6, as shown in Figure 3a, and widespread roof caving in transport roadway No.7, as shown in Figure 3b. Therefore, the stability control of roadways in broken rock mass sections is explored to propose more effective support patterns for safe roadway traffic.

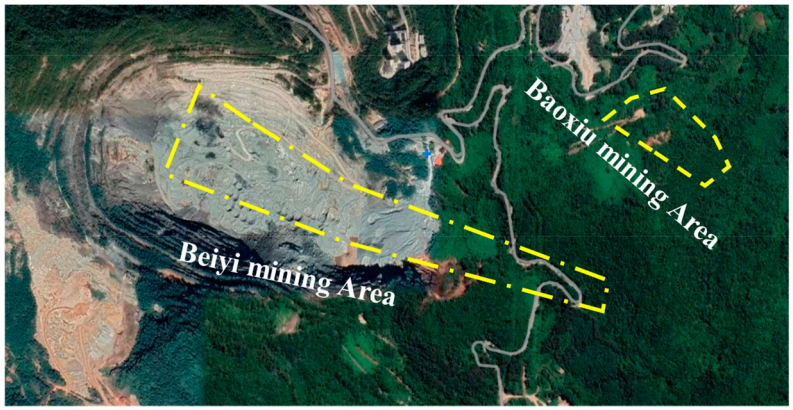


Figure 1. The area of Shilu iron deposit.

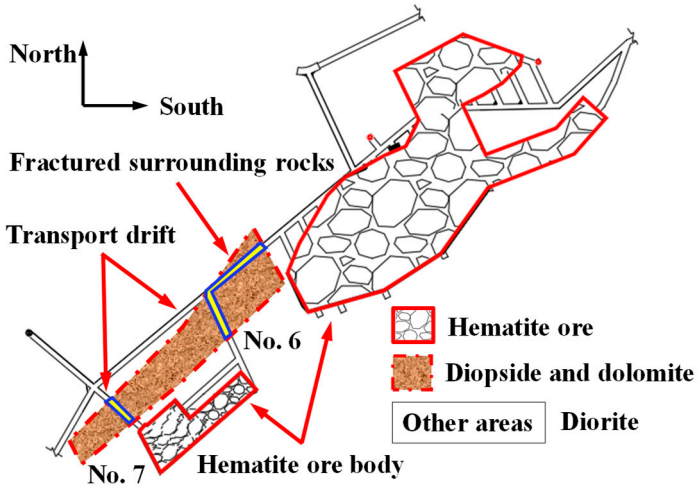


Figure 2. Engineering layout and lithology distribution.

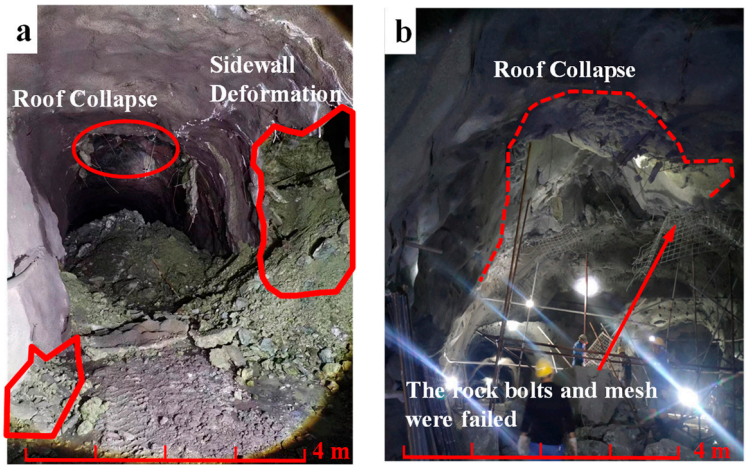


Figure 3. Support failure of broken surrounding rocks: (**a**) transportation roadways No.6; (**b**) transportation roadways No.7.

3. Quality Grade Survey of Surrounding Rock Mass

3.1. Basic Physical and Mechanical Properties of Ore Rocks

Drilling and coring operations were conducted, focusing on the surrounding rocks of No.6 and No.7 transportation roadways in the middle section of the Baoxiu-120 district at Shilu Iron Deposit. Core samples were primarily taken from the fractured surrounding

rock within a range of 5 m from the roadway walls (Figure 2). These operations addressed the stability issues of broken roadway surrounding rocks. Thirty rock cores with a diameter of 50 mm and a height of 100 mm were prepared for a series of mechanical tests. These tests included uniaxial compression, compression resistance, and shear resistance, and they were conducted to determine the basic physical and mechanical properties of the ore rock. The test results provided basic rock mass index data for subsequent rock mass quality grading, support design, and numerical simulation of surrounding rock stability. First, the rock density was measured by the quantitative product method, revealing an average core density of 2189 kg/m^3 at Shilu Iron Deposit. Second, the internal friction angle of the rock was determined to be 24.1, and the cohesion was found to be 9.59 MPa through shear testing. Table 1 lists the tensile and compressive strengths of the samples by mechanical tests.

Table 1. Tensile and compressive strengths of samples.

NO.	Location	Uniaxial Compressive Strength σ_1 (MPa)	Tensile Strength σ_2 (MPa)
1	No.6 transportation roadway in the middle section of the Baoxiu-120 district	26.77	1.5
2	No.7 transportation roadway in the middle section of the Baoxiu-120 district	15.88	1.2

3.2. Geomechanical Grading of Rock Mass

Rock mass geomechanics is graded by comprehensively considering compressive strength, rock quality designation (RQD), weathering and metamorphic characteristics, joint spacing, continuity, strike, and dip. The total score of these indicators is used as the rock mass rating (RMR) to assess the rock mass stability. Macías et al. [15] analyzed the stability of the slope located on Apollo Ramirez Boulevard, Modesto. The RMR is used to obtain the rock mass quality and the stability of the slope. This method is also applicable to support engineering in underground roadways.

$$RMR = R_1 + R_2 + R_3 + R_4 + R_5 + R_6, \quad (1)$$

$$IRMR = RMR + R_7 = R_1 + R_2 + R_3 + R_4 + R_5 + R_6 + R_7, \quad (2)$$

where R_1 is the grade of tensile strength; R_2 is the grade of RQD; R_3 is the grade of joint spacing; R_4 is the joint condition; R_5 is the groundwater condition; R_6 is the correction coefficient for the negative impact of joint direction on the process; and R_7 is the ground stress correction added by international rock mass rating (IRMR).

The average joint spacing is determined based on the survey data of rock mass joints within Shilu Iron Deposit. The accuracy of R_3 is evaluated using Equation (4). The RQD of broken rock mass is obtained according to the results of on-site drilling and coring (Figure 4).

The RQDs of No.6–7 transportation roadways in the middle section of Baoxiu-120 are 16.31% and 14.42%, respectively. The RQD scoring values are calculated using Equation (3) according to the RQD at different locations. The RQD can be obtained by the RMR evaluation system based on the experimental data of rock mechanics. Table 2 lists the relevant parameters and scoring values:

$$R_2 = 0.0012I_R^2 + 0.0692I_R + 1.23, \quad (3)$$

$$R_3 = 3.5411lnJ_v + 16.6617, \quad (4)$$

where I_R is the ROD of the rock; J_v is the joint spacing of the rock, m.

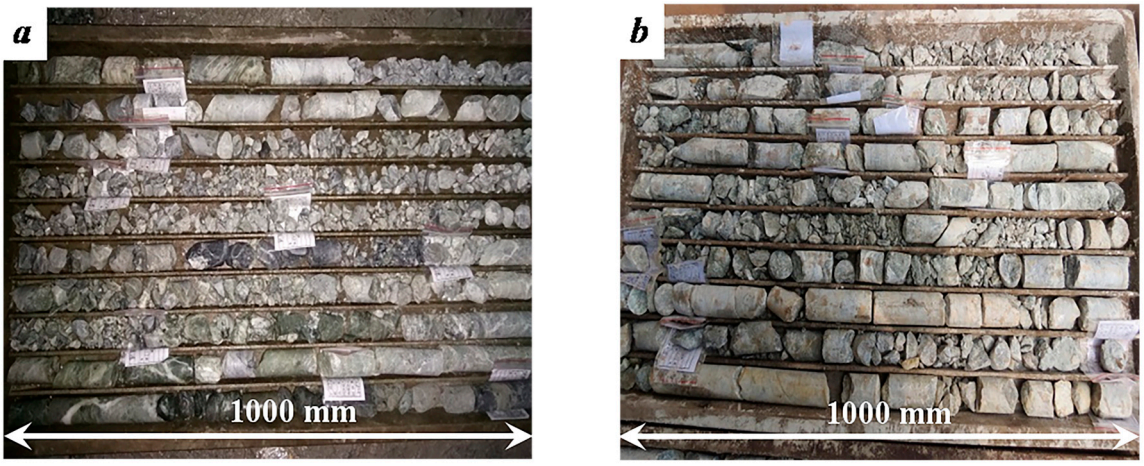


Figure 4. On-site drilling and coring: (**a**) No.6 transportation roadway; (**b**) No.7 transportation roadway.

Table 2. Relevant parameters and scoring values.

No.	Uniaxial Compressive Strength σ_1 (MPa)	R_1	RQD	R_2	Joint Spacing (m)	R_3
1	26.77	4	16.31	2.68	0.12	9.15
2	15.88	2	14.42	2.48	0.09	8.13

The RMR of the structural surface, groundwater, and joint cracks are determined according to the investigation of the structural surface, joint cracks, and ground stress in the deep part of Shilu Iron Deposit (Table 3).

Table 3. Evaluation results by IRMR.

No.	R_1	R_2	R_3	R_4	R_5	R_6	R_7	*IRMR*	Rock Mass Grading	Quality Description
1	4	2.68	9.15	10	10	−10	−4.68	21.15	IV	Poor rock mass
2	2	2.48	8.13	8	10	−5	−3.87	21.74	IV	Poor rock mass

The surrounding rocks of No.6 and No.7 transportation roadways in the middle section of the Baoxiu-120 district within Shilu Iron Deposit are classified as poor rock mass, Grade IV, according to the quality evaluation results by IRMR, as well as rock mass grading and evaluation by RMR (Table 4).

Table 4. Rock mass grading and evaluation by RMR.

Rating	<20	21~40	41~60	61~80	81~100
Quality grading Quality description	V Worse rock mass	IV Poor rock mass	III Ordinary rock mass	II Good rock mass	I Better rock mass

3.3. Selection of Support Patterns Based on Rock Quality Grading

Dangerous rocks are present on the roadway surface due to the compromised structural integrity of the deep roadway, as indicated by the deformation characteristics and survey findings. Shotcrete is employed to reinforce the surrounding surface rocks, preventing weathering and falling, and providing essential support for the roadway. While shotcrete effectively stabilizes the surface rock mass, it is insufficient for deeply fractured

surrounding rocks. To adequately address the varying support requirements, it is crucial to implement support systems that strengthen both shallow and deep rock masses. The support for shallow rock typically involves surface treatments, such as shotcrete and mesh, which focus on preventing immediate rock fall. In contrast, deep rock stabilization requires more robust solutions, such as anchor bolts used in anchor net supports that extend deeply into the surrounding rock. This approach directly enhances the stress distribution within the surrounding rocks, particularly for those with complex structural surfaces. By recognizing and addressing the differences in support needs between shallow and deep rock masses, we can ensure a safer and more stable underground environment.

Under the reinforcement of the anchor bolts, the deep surrounding rock within the reinforcement range forms a structure similar to a load-bearing arch. At the same time, the surface metal mesh encapsulates the roadway surface, providing surface support and playing a crucial role in supporting the surrounding rock in the tensile stress zones between the anchor bolts. The overall support effect is further enhanced by reinforcing the system with double ribs and pallets. Bieniawski proposed a series of support rules based on the classification of geological mechanics, tailored for the selection of support systems in roadways (Table 5). Locally broken mines and rock mass for the level-IV surrounding rocks require support through anchor nets or anchor net spray. Rock supports for No.6 and No.7 transportation roadways in the middle section of the Baoxiu-120 district at Shilu Iron Deposit adopt anchor net spray according to the support guidelines and on-site situation. Wisnuaji et al. [16] evaluated rocks in the Pelosika Dam tunnel project using the RMR method, categorizing them as inferior. The appropriate excavation sequence involves the heading excavation step method and the multiple-incremental hole drilling method. The vaults and walls are supported by anchor bolts installed in the system, made of medium and light steel ribs, reinforced by steel mesh and shotcrete.

Table 5. Rock mass quality grading and support forms.

Rock Mass Quality Grading	II	III	IV	V
Support forms	Plain spray or single anchor	Bolt-shotcrete or bolt-mesh	Anchor mesh spray	Combined support
Range of application	Unstable roadway engineering or roadways with a short service life	Locally fractured ore body or rock mass	Partially broken roadways and large-section roadways with long service life and poor stability	Severely broken roadways and unstable roadways against safe operation

3.4. Design of Roadway Support Parameters in Broken Rock Mass Areas

3.4.1. Shotcrete Support Design

The critical aspect of the concrete design is to determine the thickness of the spray layer based on the survival conditions of the deep roadway in Shilu Iron Deposit. Shotcrete supports prevent dangerous rocks from falling, which maintains roadway stability. Therefore, the thickness of shotcrete is determined based on the stability of these dangerous rocks. In other words, the bond strength of the concrete should surpass shear strength. The thickness can be calculated using Equation (5):

$$T = \frac{GK}{0.75R_tS}, \quad (5)$$

where T is the thickness of the spray layer, m; G is the gravity of the dangerous rock, N; K is the full coefficient (generally, K = 3); S is the circumference of the contact surface between the dangerous rock and the spray layer, m; and R_t is the tensile strength of the spray layer, Pa.

Radius Rr of the broken ring is calculated according to the block caving theory (Equation (6)) [17].

$$R_r = R_0 \left[(1 - \sin \varphi_0) \frac{\gamma_1 Z + c_0 \cdot ctg\varphi_0}{c_0 \cdot ctg\varphi_0} \right]^{\frac{1-\sin\varphi_0}{2\sin\varphi_0}}, \quad (6)$$

where γ_1 is the bulk weight of the overlying rock formation (weighted average); Z is the distance from the roadway center to the surface, m; c_0 is the adhesion of the rock, N; φ_0 is the internal friction angle of the rock, °; and R_0 is the radius of the outer circle of the roadway, m.

The top pressure per meter of roadway is calculated (Equation (7)) [17]:

$$Q_d \approx 2a \cdot \eta (R_w - h)\gamma, \quad (7)$$

where a is half of the upper width of the roadway excavation section, m; η is the correction coefficient of roadway width; R_w is the radius of the surrounding rock crushing ring, m; h is the height from the circle center to the roof, m; and γ is the bulk weight of the roof rock, kg/m^3.

The roof pressure per unit area is calculated (Equation (8)) [17]:

$$q_d = \frac{Q_d}{2a} = \gamma \cdot \eta (R_p - h). \quad (8)$$

The internal friction angle of the two overburden rock masses is 24.1° at the top and bottom of the roadway; the average bulk weight of the overburden rock formation γ = 2.70 t/m^3; the radius of the three-centered arch of the roadway R_0 = 2.47 m; and h = 2.13 m. According to Equation (6), crushing ring's radius R_p = 4.16 m; roadway's roof pressure q_d = 7.18 t/m^2; and Q_d = 0.18 MPa.

The thickness of the sprayed shotcrete layer in Shilu Iron Deposit is calculated to be 53.02 mm and determined as 55 mm using Equation (8) when G = 15 kN and the roadway roof is almost load-free.

The shotcrete parameters of Shilu Iron Deposit align with standard support specifications. Wet concrete injection machinery is used for shotcrete application. The raw materials consist of Portland cement, medium-fine sand with particles smaller than 2.5 mm, and stones no larger than 15 mm. These components are mixed in a weight ratio of 1:2:2. The water–cement ratio is between 0.3 and 0.4. A quick-setting agent is added at 3–5% of concentration to optimize coagulation.

3.4.2. Parameter Design of Anchored Mesh Supports

The bolt diameter, length, spacing, and arrangement are optimized according to the geological conditions and on-site deformation measurement of the surrounding rock of the roadways in Shilu Iron Deposit. Surrounding rocks can remain stable under the anchored mesh support. Resin bolts consolidate the anchoring end of the bolt with the broken rock mass of the hole wall, which creates a cohesive unit through cementation. They exhibit superior shear and tensile strengths compared to other bolts. Therefore, resin bolts are employed. A rectangular metal mesh with dimensions of 80 mm by 80 mm is used. The parameter design of anchored mesh support involves bolt length, diameter, spacing, and anchoring depth.

(1) Calculation and Determination of the Bolt Length

The bolt length is calculated as in Equation (9):

$$L \geq L_a + L_b + L_c \lim_{x \to \infty}, \quad (9)$$

where L is the bolt diameter, m; L_a is the exposed part of the bolt (L_a = 0.10 m); L_b is the effective length of the bolt (Pressure-free arch height h is taken for the roof bolt), m; and L_c is the total length of the anchor (L_c = 0.6 m).

The effective length of the bolt is consistent with the radius of the crushing zone of the surrounding rocks, which ensures optimal support effect. The radius of the crushing zone of the roadway roof can be considered equivalent to the height of the caving zone (L_b = h). The height of the caving zone is calculated to be 1.45 m using Equation (10) for goafs with spans less than 6 m according to the parabolic pressure arch theory [18]. The bolt length is calculated to be 2.15 m and subsequently rounded up to 2.2 m.

$$h = \frac{a + b\left[ctg\alpha + ctg\left(45^\circ + \frac{\varphi}{2}\right)\right]}{f}, \tag{10}$$

where a is the length of the roadway (a = 4.5 m); b is the width of the roadway (b = 3.8 m); α is the angle between the two sides and the ground (α = 85°); φ is the internal friction angle of the rock (φ = 24.1°); and f is the stability coefficient of the surrounding rock (f = 3.16).

(2) Row and Column Spacing Design

Bolts are arranged in an even pattern with uniform spacing both in rows and columns. The bolt spacing is calculated to be 1.08 m and rounded to 1.1 m using Equation (11), considering the weight of rocks suspended by each bolt.

$$a = \sqrt{\frac{Q}{K\gamma L_2}}, \tag{11}$$

where a is the spacing of the bolt, m; Q is the anchoring force determined by the tensile test, kN; γ is the average bulk weight of the surrounding rock (γ = 28.0 kN/m^3); and K is the safety coefficient of the bolt (K = 2.0).

(3) Design of Bolt Diameters

Bolt diameter d is expressed as Equation (11) based on the strength principles of bearing and anchoring force. It is calculated to be 19.6 mm and rounded to 20 mm.

$$d = 35.52\sqrt{\frac{Q}{\sigma_t}}, \tag{12}$$

where d is the bolt diameter, mm; Q is the anchoring force determined by the tensile test, kN; and σ_t is the tensile strength of the bolt material, MPa.

The surrounding rocks of the transportation roadways in the middle section of Baoxiu-120 is re-supported according to the above support structure and parameters (Figure 5). The roadway exhibits an optimal support effect without issues such as roof caving, rib spalling, and damage to the bottom corners.

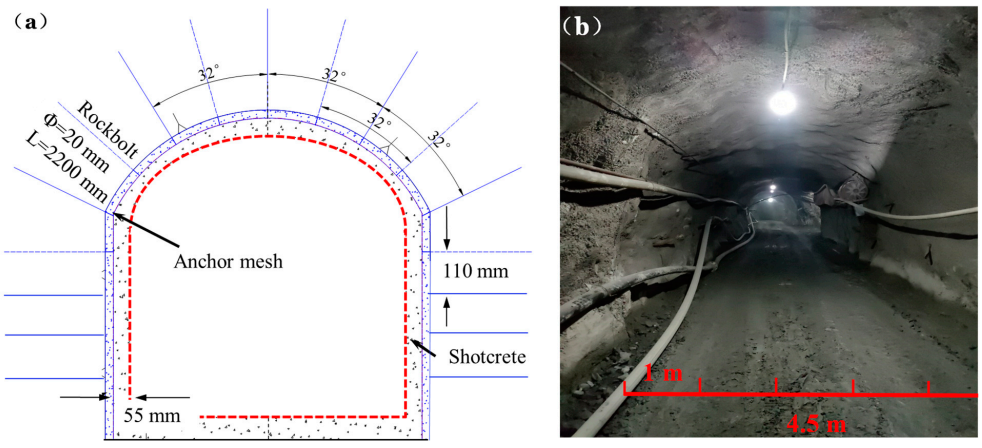


Figure 5. Support design and effect: (**a**) support design; (**b**) supported roadway.

4. Engineering Applications and Discussion

The cross-section deformation law of the roadway's surrounding rocks is analyzed to understand the deformation failure characteristics of the supported roadway. The displacement in the two sides of the roadway over time is analyzed using the mechanical transmission displacement monitoring method. The stability of the supported surrounding rocks is evaluated through roadway deformation. This analysis is instrumental in assessing the efficacy of support measures and in evaluating the long-term stability of the surrounding rock.

4.1. Monitoring Equipment and Layout Method

Digital convergence gauge JSS30A is used to monitor the cross-section displacement of the roadway. This equipment is manufactured by Shanghai LeiYun Testing Instruments Co., Ltd., located in Shanghai, China. The equipment installation method is shown in Figure 6. Two convergence gauges are connected to three monitoring points, A, B, and C, within the roadway. Relative displacements ΔAB and ΔBC are recorded and displayed on the digital convergence gauges to calculate roof displacement ΔCD when the distances between monitoring points (L_{AB} and L_{BC}) change. This monitoring method accurately tracks the displacement changes of the roadway's cross-section, which obtains the relative displacements between two points at different times. The anchoring bolts of the digital convergence gauges are drilled and fixed before the application of shotcrete. After that, the digital convergence gauges are installed to read data at intervals of 3–7 days.

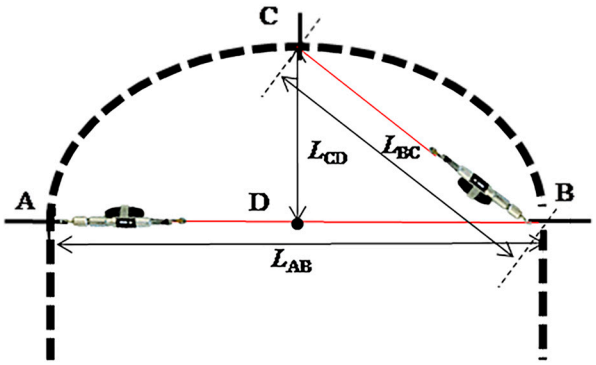


Figure 6. Deformation monitoring of roadway roof and surrounding rocks on two sides.

4.2. Discussion

Figure 7 shows the change curves of monitoring data for the displacement (D) of surrounding rocks in the cross-section of the supported roadway.

The sink rate of the roof aligns with the convergence trend in the horizontal direction (Figure 7). The surrounding rock exhibits a significant convergence deformation rate, with the deformation amount exceeding 20 mm within the first 5 days of the roadway support. The convergence rate of the two sides is 5.50 mm·d^{-1}, which is slightly higher than the sink rate of the roof. Subsequently, the convergence deformation rate rapidly decreases and stabilizes after one month. The abrupt change in the convergence rate of the surrounding rock during the initial stage can be attributed to two primary factors. First of all, the relative deformation of the rock mass increases under gravity, which increases the anchoring force of the bolts and anchor mesh in the early support stage. The deformation of rock mass is constrained only when the anchoring force of the bolts and anchor mesh is sufficiently robust. Second, the concrete sprayed on the surface of the surrounding rocks requires a certain curing duration to reach its specified strength.

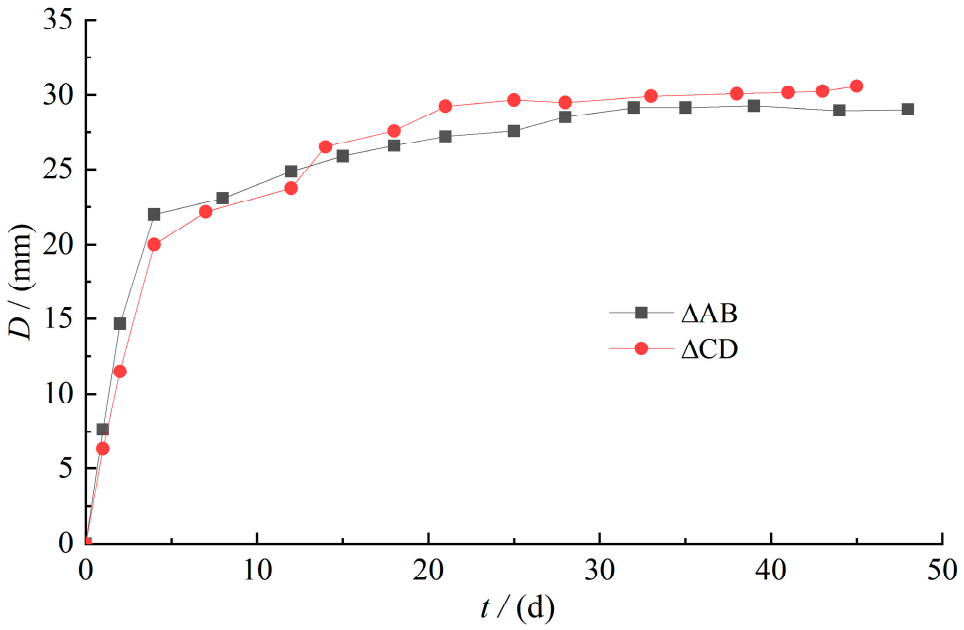


Figure 7. Displacement of roadway roof and surrounding rocks on two sides.

The initial concrete strength is directly proportional to the curing duration. Insufficient concrete strength can lead to localized deformation of the rock mass prior to complete solidification. As support time progresses, the surrounding rocks undergo certain displacements. Concurrently, the strength of the concrete and the anchoring effect of the bolts and mesh rapidly increase, which ultimately enhances the strength of the surrounding rocks in the anchoring zone.

The behavior of the rock mass is influenced by changes in stress distribution within the rock, which evolves in response to the applied support. After one month, the deformation of the surrounding rocks is controlled, with displacements of the roof and horizontal sides confined to less than 35 mm. This indicates that the joint support pattern effectively meets the stability requirements of the surrounding rocks.

Subsequent investigations confirm that the adoption of this integrated support approach for the roadway in this section has successfully prevented rib spalling and roof caving. The cross-section of the roadway maintains its original state, ensuring both stability and long-term support effectiveness. The integration of anchor bolts, anchor mesh, and shotcrete consolidates the surrounding rocks into relatively cohesive units, thereby improving their mechanical properties and resilience under stress.

This case underscores the importance of understanding the damage mechanisms during excavation. As highlighted by Costamagna et al. [19] assessing the quality of rock excavations is crucial for developing effective support solutions that enhance stability. Furthermore, Høien et al. [20] emphasize the significance of recognizing deformation characteristics and support requirements in underground settings. This comprehensive support system not only addresses immediate stability concerns but also enhances the overall behavior of the rock mass under varying rock mass quality conditions, drawing valuable lessons from existing literature on rock excavation and support practices.

5. Conclusions

In the No.6 and No.7 transportation roadways of the middle section of Baoxiu-120 at the Shilu Iron Deposit, significant rock mass failures, including roof caving and rib spalling, were observed. A comprehensive assessment classified the rock mass in this section as level IV based on data obtained from field investigations, structural surface analyses, drilling activities, and laboratory rock experiments.

Informed by this evaluation and the support guidelines derived from geomechanical classification methods, a joint support system comprising anchor mesh and shotcrete was implemented. The design parameters for the support structure at Shilu Iron Deposit were established as follows: the shotcrete was applied with a thickness of 55 mm, using a mix of Portland cement, medium-fine sand (with particle sizes smaller than 2.5 mm), and stones (with particle sizes smaller than 15 mm) in a weight ratio of 1:2:2. The water–cement ratio was maintained between 0.3 and 0.4. Additionally, resin bolts with an outer diameter of at least 20 mm and a length of 2200 mm were employed, with row and column spacings set at 1100 mm. A rectangular metal mesh with dimensions of 80 × 80 mm served as the anchor mesh. Digital convergence gauges were utilized to monitor deformations within the roadway. In the initial five weeks following the implementation of the support system, significant changes in convergence deformation rates were recorded, with displacements exceeding 20 mm at the sides and roof of the roadway. However, after one month, the convergence deformation rates rapidly decreased and stabilized. The adopted support patterns effectively controlled displacement and mitigated stress concentration within the surrounding rocks, thereby ensuring the overall stability of the roadway.

This case highlights the importance of conducting thorough rock mass quality assessments prior to support design. The timely recognition of changes in rock mass quality and the subsequent redesign of support structures are critical for maintaining stability in underground environments. By integrating continuous monitoring and adaptive design practices, we can enhance the safety and effectiveness of support systems in similar geological settings.

Author Contributions: Methodology and visualization, C.M., P.W. and J.L.; writing—original draft preparation, C.M., P.W., J.L. and X.F.; writing—review and editing, Z.D., Z.C., X.F. and X.W. All authors have read and agreed to the published version of the manuscript.

Funding: This work was financially supported by the National Key R&D Program of China (No. 2023YFC2907400, 2021YFC2900500), the Hainan Province Science and Technology Special Fund (ZDYF2024GXJS307), and the National Natural Science Foundation of China (No. 52074020).

Data Availability Statement: The original contributions presented in this study are included in the article. Further inquiries can be directed to the corresponding author.

Acknowledgments: We acknowledge the valuable advice of the editors and reviewers.

Conflicts of Interest: Author Xingwu Wang was employed by the company Hainan Mining Co., Ltd. The remaining authors declare that the research was conducted in the absence of any commercial or financial relationships that could be construed as a potential conflict of interest.

References

1. Wen, Q.P.; Hao, Z.; Qi, W.; Gang, P. Study on Safety Control of Large-section Roadway with High Stress and Broken Surrounding Rock. *Adv. Civ. Eng.* **2021**, *2021*, 6686208. [CrossRef]
2. Zhang, C.X.; Guo, J.F.; Yuan, Y. The Current Status and Prospects of Mining Technology for Complex Ore Bodies in Metallurgical Mines in China. *Min. Technol.* **2006**, *3*, 8–10+29. (In Chinese) [CrossRef]
3. Pan, R.; Lei, W. Experimental Study on the Bearing Behavior of Bolted and Grouted Broken Surrounding Rock of Deep Roadways in a Coal Mine. *KSCE J. Civ. Eng.* **2024**, *28*, 4032–4040. [CrossRef]
4. Lee, J.; Rehman, H.; Naji, A.M.; Kim, J.J.; Yoo, H.K. An Empirical Approach for Tunnel Support Design through Q and RMi Systems in Fractured Rock Mass. *Appl. Sci.* **2018**, *8*, 2659. [CrossRef]
5. Yu, W.J.; Qu, Y.S.; Deng, D.Q. Supporting Numerical Simulation of Roadway Surrounding Rock in Deep High Stress Based on Broken-expand Deformation. *Appl. Mech. Mater.* **2013**, *2545*, 1310–1314. [CrossRef]
6. Huang, J.H.; Wei, X.Q.; Luo, Y.; Gong, H.L.; Liu, T.T.; Li, X.P. Analysis of the Deformation Characteristics of the Surrounding Rock Mass of a Deep Tunnel During Excavation Through a Fracture Zone. *Rock Mech. Rock Eng.* **2022**, *55*, 7817–7835. [CrossRef]
7. Huang, X.; Li, S.Y.; Jin, J.H.; Shi, C. Determining Digital Representation and Representative Elementary Volume Size of Broken Rock Mass Using the Discrete Fracture Meshwork–discrete Element Method Coupling Technique. *Appl. Sci.* **2024**, *14*, 606. [CrossRef]
8. Zhao, X.D.; Zhu, Q.K.; Westmanb, E.; Yang, S.H. Research on Failure Mechanism and Support Technology of Fractured Rock Mass in an Undersea Gold Mine. *Geomat. Nat. Haz. Risk.* **2023**, *14*, 2221776. [CrossRef]

9. Niu, Q.J.; Jiang, L.H.; Wu, C.L.; He, X.; Li, C.; Wang, X.Z.; Zhang, Z. Numerical Analysis on Fractured Roadway Stability Based on the Fdm–Dfn Coupling Method. *Int. J. Geomech.* **2024**, *24*, 04024204. [CrossRef]
10. Yu, X.J.; Yang, Y.P.; Li, X.F.; Luo, H.Z.; Wang, Y.S.; Zhang, X.Z.; Kou, Y.Y.; Li, H.Y.; Zhou, Y.Y. Cracking Formation and Evolution in Surrounding Rock of a Deep Fractured Rock Mass Roadway: A Study of the 790-M Level Segment Engineering at the Jinchuan Mine, China. *Eng. Geol.* **2024**, *331*, 107431. [CrossRef]
11. Yao, G.H.; Wu, A.X.; Wang, H.J.; Du, Z.J. Optimization of Spray Anchor Support Parameters and Process Research in Soft and Fractured Rock Tunnels. *China Min.* **2010**, *19*, 70–74. (In Chinese)
12. Zhou, G.J.; He, Y. Research on the Joint Support Mechanism of Weak Rock Mass Based on Flac-(3D) Numerical Simulation. *Non-Ferr. Min. Metall.* **2019**, *35*, 6–10. (In Chinese)
13. Zhang, T.; Li, J.M.; Guo, S.M.; Liu, T. Optimization of Support Parameters for Fractured Rock Mass Tunnels in Deep Copper Mines. *Min. Metall.* **2019**, *28*, 17–21. (In Chinese) [CrossRef]
14. Yang, Y.P.; Yang, Y.L.; Mu, Y.S.; Han, B. Research and Application of Deep High-stress Fractured Rock Roadway Support Technology in Jinchuan Mining Area. *China Min.* **2018**, *27*, 99–103. (In Chinese) [CrossRef]
15. Macías, A.M.; Ver, D.K.; Borja, C.P.; Bordehore, L.J. Stability Assessment of Rock Slopes Combining Slope Mass Rating and Qslope Classification Systems: A Case Study in Cerro San Eduardo (Guayaquil, Ecuador). *IOP Conf. Ser. Earth Environ. Sci.* **2021**, *833*, 981–985. [CrossRef]
16. Wisnuaji, H.; Setiawan, H.; Setiawan, N.I. EXCASS System and Rock Mass Rating (RMR) Classification for Determining Excavation Method and Tunnel Support at Pelosika Dam Spillway Tunnel. *IOP Conf. Ser. Earth Environ. Sci.* **2023**, *1233*, 012008. [CrossRef]
17. Wang, X.F.; Cai, Z.Q. *Design of Support in Underground Engineering*; Science Press: Beijing, China, 2016. (In Chinese)
18. Ding, X.; Liu, Y.; Han, Z.M.; Zhang, J.D.; Fan, H.B.; Tian, Y.; Ma, K.M. Study on Surrounding Rock Pressure of Deep Jointed rock Tunnel Based on Pressure Arch Theory. *J. Hebei Univ. Sci. Technol.* **2024**, *45*, 434–442. (In Chinese)
19. Costamagna, E.; Oggeri, C.; Vinai, R. Damage and Contour Quality in Rock Excavations for Quarrying and Tunnelling: Assessment for Properties and Solutions for Stability. *IOP Conf. Ser. Earth Environ. Sci.* **2021**, *833*, 012137. [CrossRef]
20. Høien, T.; Løken, Ø.; Mæhlum, H. Main Aspects of Deformation and Rock Support in Norwegian Road Tunnels. *Tunn. Undergr. Space Technol.* **2019**, *86*, 262–278. [CrossRef]

Disclaimer/Publisher's Note: The statements, opinions and data contained in all publications are solely those of the individual author(s) and contributor(s) and not of MDPI and/or the editor(s). MDPI and/or the editor(s) disclaim responsibility for any injury to people or property resulting from any ideas, methods, instructions or products referred to in the content.